Tri-stable Electrochromism with Passive Radiative Cooling for Year-Round Building Energy Saving

Zewei Shao[1,2,#], Aibin Huang[1,2,#], Cuicui Cao[1,2,#], Xiaowei Ji[1,2], Wei Hu[1,2], Hongjie Luo[3], John Bell[4], Ping Jin[1,2] , Ronggui Yang[5,*] and Xun Cao[1,2,*]

[1]State Key Laboratory of High-Performance Ceramics and Superfine Microstructure, Shanghai institute of Ceramics, Chinese Academy of Sciences, Dingxi 1295, Changning, Shanghai, 200050, China.

[2]University of Chinese Academy of Sciences, Beijing, 100049, China.

[3]Institute for the Conservation of Cultural Heritage, Shanghai University, Shanghai, 200444, China

[4]Office of the Deputy Vice-Chancellor(Research and Innovation), Research and Innovation Division, University of Southern Queensland, Australia

[5]State Key Laboratory of Coal Combustion, School of Energy and Power Engineering, Huazhong University of Science and Technology, Wuhan, Hubei 430074, China.

#These authors contributed equally to this work.

*Corresponding Authors: cxun@mail.sic.ac.cn (X.C), ronggui@hust.edu.cn (R.Y.)

Abstract:

Building energy consumption for heating and cooling is a critical issue that has garnered wide attention due to its significant impact on global warming and sustainability. In particular, windows account for >20% of building energy loss. There is an urgent need for the independent optimization of thermal radiative properties of windows for tri-band radiation, including visible, near-infrared (NIR), and mid-infrared (MIR). Here we develop a new electrochromic structure for thermal management of windows, which is able to maximize the utilization of both solar radiation of visible and NIR light and radiative cooling of MIR light. We propose a tri-stable electrochromic device (ECD) based on the phase transitions of VO_2 and WO_3 films. The VO_2-WO_3 based ECD could realize three different optical states to independently regulate visible and NIR transmittance. Due to the decoupled barrier for opaque state in rutile Li_xVO_2, our device also maintains non-volatility and tri-stability (<10% bleaching over 4 hours). Moreover, we introduce a new approach for thermal regulation by optimizing the emissivity of outside ($\varepsilon_{MIR\text{-}O}$ of 0.79) and inside ($\varepsilon_{MIR\text{-}I}$ of 0.33) electrodes to minimize radiative heat exchange between the indoor and outdoor environments. Outside experiments were performed in Sanya, China, realizing continuous all-day cooling of ~2-8 °C compared to low-e windows on a typical clear sunny day at Southern China latitudes. Simulation shows that this new ECD exhibits a higher heating and cooling energy savings than a commercial low-E glass in most climates around the world. Our findings render great opportunities for the innovative energy-saving window designs that can help achieve global carbon neutrality and sustainability.

Introduction

Buildings are responsible for about 40% of total the U.S. energy use, of which about 40% is directly related to the operation of heating, ventilation and air-conditioning (HVAC) systems.[1-3] Windows, as the primary means of energy exchange between the interior and exterior environments, play a crucial role in building energy consumption, accounting for as much as 20% of HVAC energy loss.[4] The energy exchange through windows is quite complex involving conduction, convection and thermal radiation. The thermal radiation energy exchange is broadband, mainly composed of solar heating in the visible (380-780 nm) and near-infrared (NIR, 780-2500 nm) wavelength ranges, the spontaneous emission in the mid-infrared (MIR, 8-13 μm) wavelength range, and also indoor lighting depending on the visible transmittance.[5-7] To reduce building energy consumption and improve lighting utilization at complex environment conditions, a comprehensive optimization of spectrum from visible to MIR wavelength range is often necessary.[8-9] However, the separate optimization for the wavelength ranges of visible, NIR, and MIR in windows has been rarely studied.

Electrochromic (EC) smart windows, which can dynamically regulate solar radiation under external voltage stimuli, have been regarded as a promising technology to reduce the building energy consumption and to enhance thermal comfort.[10-12] To balance of indoor daylight and heat exchange, dual-band EC smart windows are a recent technology which can improve the building energy efficiency via the dynamic and independent control of NIR and visible light transmittance.[13-15] Additionally, the optimization of thermal emission in MIR range is also important to minimize radiative heat exchange between the indoor environment of buildings and the outdoor environment.[16-18] However, traditional electrochromic devices usually require glass substrates in both the front and back sides for the growth of the transparent ITO electrodes and also maintaining structural integrity. Glass substrates usually have a high emissivity over the MIR range.[19,20] To provide EC devices with the optimization of energy between inside and outside environment, new EC structures with MIR radiative property regulation have been demonstrated to reduce the energy consumption.[21,22] These tuning electrochromic processes focused on the solar heating or thermal emissivity, and it would still be challenging to develop wider and independent thermal management over the spectrum from visible to MIR wavelength range.

In this study, for reducing the building energy consumption, EC windows are developed, which adapts thermal radiative properties for visible, near-infrared (NIR), and mid-infrared (MIR) according to the environment conditions involving changes in temperature and solar irradiation. By adding external voltage to control the Li-doping depth in a VO_2-WO_3 electrochromic structure, we tuned non-volatile and reversible phase transitions of monoclinic-VO_2/rutile-H_xVO_2[23-25] and monoclinic-WO_3/cubic-Li_yWO_3[26-27] (Supplementary Figs. 1-2), to regulate the solar irradiation in the NIR and visible regions. The structure design of quartz-ITO/WO_3/VO_2/electrolyte/ITO-PE improves the energy-saving performance of ECD. This structure features high-emissivity quartz substrate on outdoor side and low-emissivity ITO/PE on inner side, which can minimize radiative heat exchange between the indoor and outdoor environments, thus saving energy for all-year cooling and heating while satisfying the lighting requirement without reducing the aesthetical effect.

Results

Tri-band optimization of ECD

According to the solar spectrum and the MIR thermal radiation spectrum around room temperature, we proposed a set of characteristics for an ideal EC window (**Fig. 1a**) that can maximize the utilization of the tri-band radiation of visible, NIR and MIR light. The visible and NIR lights heat the internal objects, and the visible light will also significantly affect the internal lighting. Independent regulation of the visible and NIR lights according to different weather conditions is therefore desirable. Furthermore, to reduce heat-exchange flux (P_{exchange}) in ambient condition, an ideal smart window requires low-emissivity substrate on the inner side, which can help minimize radiative heat exchange between the indoor and outdoor environments, thus saving energy for all-year cooling and heating. Unlike the emissivity modification achievable on the inner side of windows, due to safety and operational stability requirements, the outer side of windows necessitates rigid substrates, which exhibit high emissivity. Notwithstanding this, high emissivity on the outer side readily enables passive radiative cooling in hot environments, thereby achieving energy savings.

For the regulation for solar irradiation, a VO_2-WO_3 electrochromic structure is adopted (**Fig.**

1b). By adding external voltage to control the Li-doping depth, we tuned non-volatile and reversible phase transitions of monoclinic-VO_2/rutile-H_xVO_2 and monoclinic-WO_3/cubic-Li_yWO_3, which correspond to the regulations of NIR and visible regions. To realize low-emissivity on the inner side, we design a new structure by replacing inner side glass substrate with an IR-transparent PE film. The low-emissivity effect thereby can be realized by the high MIR reflectance of ITO films. We selected 0.1mm-PE/ITO and 0.05mm-PE/ITO as representative samples and compared it with the front and back side of commercial ITO/Quartz film (labeled as ITO/Quartz and Quartz/ITO). As illustrated in **Fig. 1c**, four sample films were placed on the same hot plate (40 °C). The thermal images after temperature stabilization exhibited a notable difference (**Fig. 1d**). The Quartz/ITO sample demonstrated very high emissivity in the MIR range (2.5μm-15μm, ε: ~0.79). Hence, it was shown to have a high surface temperature under the thermal camera. In contrast, 0.05mm-PE/ITO film appeared much colder, which is closed to the low-emissivity ITO/Quartz sample (0.05mm-PE/ITO: ~0.33, 0.1mm-PE/ITO: ~0.44, ITO/Quartz: ~0.26, Supplementary Figs. 3-6), revealing the lower heat radiation. Meantime, the optical and electrical performance of 0.05 mm-PE/ITO films (Rs= 23 ohm/sq, $T_{\text{vis-NIR}}$=76.5%) are very close to that of commercial ITO/Quartz films (Rs= 17 ohm/sq, $T_{\text{vis-NIR}}$=81.1%).

Therefore, the indoor and outdoor sides of the device were set constantly as low-emissivity 0.05mm-PE substrate ($\varepsilon_{\text{MIR-I}}$ of 0.33) and high-emissivity quartz substrate ($\varepsilon_{\text{MIR-O}}$ of 0.79). This device was composed of quartz-ITO/WO_3/VO_2/SPE/ITO-PE, namely, tri-band optimized EC device for future investigation in below text. As shown in **Fig. 1e**, the fabricated tri-band optimized ECD could independently regulate the visible and NIR lights, exhibiting obvious three different optical states as mentioned: bright, cool and dark (More details about the spectrum in visible-NIR range are given in Supplementary Figs. 7-9), and the front and back sides of the device show significantly different MIR emission (~0.33 and ~0.79) in the wavelength range of 2.5-20 μm. Such an optical performance in the spectral characteristics of the device is the three states, which lays the foundation for thermal management energy-saving.

Fabrication and characterization

Fig. 2a shows the schematic of the ECD (quartz-ITO/WO_3/VO_2/electrolyte/ITO-PE). The

ECD was manufactured by sputtering WO_3 and VO_2 films, followed by an extra electrolyte layer containing $LiClO_4$ and ferrocene. Here, we select ~40 nm VO_2 as NIR-regulated layer, which could be enough meeting daylighting (luminous transmission, T_{lum} ~55%), and be able to regulate the solar transmittance effectively (solar modulation ability, ΔT_{sol} ~7%). More details about the preparation and structure characterization are given in the Experimental section and Supplementary Figs. 10-13. Electrochromic properties of the ECDs were measured *in-situ*. The optical transmittance spectra (**Fig. 2b**) of Li^+ intercalation/deintercalation of the VO_2/WO_3 ECD indicate an excellent dual-band electrochromic performance, certifying that VO_2 is effective as an NIR selecting layer for electrochromic applications. A dual-band modulation process over the solar spectrum can be converted from the transmittance spectra, as shown in **Fig. 2c**. Specifically, the VO_2/WO_3 ECD can be switched over three different optical states by varying the applied voltages. At +1.5 V ~ 0 V, the device is transparent to both visible and NIR light (bright state). At 0 ~ -1.5 V, the VO_2 layer was intercalated into Li^+ and the cool state is activated where the device blocks most of the NIR (Transmittance at 1500 nm: 55.5% at 0 V, 16.4% at -1.5 V) while maintaining a good visible light transmittance (Transmittance at 670 nm: 58.6% at 0 V, 50.4% at -1.5 V). When the applied voltage is continuously reduced to -3.5 V, the device switches to the dark state where it blocks 94.2% of 670 nm visible light and 96.6% of 1500 nm light. The optical transmittance spectra were converted to the visible illumination and NIR heat in Supplementary Fig. 14 and Table S1 to show the expected performance in solar irradiation modulation. In the cool state (-1.5 V), the film blocks 76.4% of the solar heat in the NIR region while maintaining a high visible light transmittance of 46.8% for daylighting. The cool state can therefore reduce significantly the building energy use on air conditioning and lighting. For a growing command for blocking visible light, at -3.0 V (dark state), the film exhibits an aesthetically pleasing dark blue color and blocks 92.7% of total solar energy.

The phase transitions induced from ion gating were also detected by *ex-situ* XRD, as shown in **Fig. 2d**. The VO_2/WO_3 films were fully de-intercalated at pristine condition, exhibit pristine monoclinic phases of both VO_2 and WO_3. With the ion intercalating, the presence of Li_yWO_3 were confirmed by the peak change of XRD spectrum. When the voltage was decreased to -3.0 V, in contrast to the 23.1°, 23.6° and 24.4° peaks of the m-WO_2 (002), (020) and (200) planes in pristine sample, peak at 23.9° marked by blue pattern occurred, which was assigned to the

Li-induced c-Li_yWO_3 film.[28-29] When further increasing the applied voltage to +1.5 V, the typical peaks of m-WO_3 changed to their initial monoclinic structures due to the Li^+ de-intercalation. Remarkably, the typical peaks of VO_2 show no obvious change, which can be attributed to the similar crystal structure between monoclinic phase and rutile phase, as explained in previous works.[35] The Li^+-intercalation into m-VO_2 from 0 V ~ -1.5 V was confirmed by the emergence of the V^{3+} ($2p_{3/2}$) peak in XPS analysis, as shown in Supplementary Fig. 15 and Table S2. The V *2p* XPS spectrum of the pristine VO_2/WO_3 films, shows the coexistence of V^{4+}, a few V^{5+} and almost no V^{3+}. With the decrease of bias voltage, the valence shows obvious changes in V. With the intercalation of Li^+, V^{4+} was reduced progressively to V^{3+}, the presence of which was detected in the V $2p_{3/2}$ XPS spectra. The proportion of V^{3+}/V increased from 0 for pristine sample to 13% at -0.5 V, to 40% at -1.0 V and final to 60% at -1.5 V. These measurements suggest that the Li^+ intercalation of m-VO_2 is gradually increasing along the depth of films. Therefore, the dual-band electrochromic mechanism in VO_2/WO_3 films could be explainable by the model of depth diffusion. When the voltage is small, the Li^+ was firstly diffused into m-VO_2, inducing NIR regulation. And when the voltage is enough (<-3.0 V) driving the Li^+ into WO_3 layer, visible regulation was realized. Besides, real-time transmittance spectra were used to determine the regulation process and electrochromic information between different operating states (bright, cool, and dark), showing great cycle stability (<10% degradation after 1200 cycles), capacity stability (<5% capacity loss after 1200 cycles), fast switching speed (coloration to 90% in 6.2 s and bleaching to 90% in 3.1 s at 670 nm) and high coloration efficiency (123 cm^2/C at 670 nm) (Supplementary Figs. 16-18 for detail information).

We also studied the tri-stability of our device, which is the ability to maintain bright, cool and dark states without the constant application of a voltage, which is an important factor to evaluate electrochromic device. A good EC device with great tri-stability could save energy maintaining the bleaching or colored state. In our device, it can be seen from the inset of **Fig. 2e** and Supplementary Figs. 19a that, compared to bare WO_3 film, VO_2/WO_3 films based on Li^+ intercalation/de-intercalation has good optical memory retention in the three states. The bright, cool and dark state states were stable (<10%) for more than 4 h without voltage after a stimulation of +1.5 V, -1.5 V and -3.0 V for 20 s. In our device, the VO_2 and Li_xVO_2 exhibits non-volatility, which helps improve tri-stability.[31-32] With Li^+ diffusing into the VO_2-WO_3 films, the m-VO_2 would be gradually transferred into stable metallic r-VO_2, which could effectively prevent Li^+ return to electrolyte (Supplementary Fig. 19b). The main advantage of VO_2 is that the barrier for state retention is decoupled from the barrier for changing states, allowing for maintaining non-volatility, compared to WO_3 (Supplementary Figs. 19c). To understand the source of non-volatility of VO_2 layer, *ex-situ* Raman spectrum and Kelvin potential measurement were used to figure out the role of VO_2 films obstructing ion diffusion during the coloration. The Raman spectrum in Supplementary Fig. 20 shows that the typical peaks at 100-800 cm^{-1} of VO_2 disappeared as the voltage decreased to -3.0 V. This could be attributed to gradual Li^+-intercalation, leading to the maintenance of the new VO_2 phase for a prolonged duration of up to 4 hours at open circuit (OC) state. Same results could also be seen by surface potential in **Fig. 2f**, the VO_2-WO_3 films could maintain a stable surface potential state in OC state for 4 hours (median potential: 0.42 V to 0.38 V, the top **Fig. 2g**) during the coloration process. Compared to VO_2-WO_3 structure, WO_3 shows a much worse non-volatility. As shown in the bottom **Fig. 2g** and Supplementary Fig. 21, at an open circuit condition, WO_3 shows a rapid degeneration from 0.61 V to 0.32 V only after 10 min, and from 0.32 V to -0.03 V after 4 hours. In summary, by tuning non-volatile and reversible phase transitions of monoclinic-VO_2/rutile-H_xVO_2 and monoclinic-WO_3/cubic-Li_yWO_3, we obtained a tri-stable electrochromic structure with MIR optimization.

Outdoor performance

Finally, we performed a continuous experiment in a balcony at Sanya, China from 00:00 on 26 November 2022 to 23:59 on 26 November 2022 (with a clear sky and relative humidity of ~80%). As shown in **Fig. 3a**, we placed five samples (Tri-stable ECD with bright, cool, dark states, commercial Low-e glass and white glass) on the windows. As shown in **Fig. 3b**, the five temperature curves, ambient temperature and solar irradiation were recorded (complete temperature curves can be seen in Supplementary Fig. 27). The peak irradiation of sunlight was ~660 W/m^2. As expected, different states could be suitable for different weather conditions, as shown in **Fig 3c**. Before 9:00, when the solar irradiance is not yet strong (<100 W/m^2), the difference in temperature among several different windows is no more than 1°C. Considering the lighting indoor, the bright state is suitable during this time. When the solar irradiance become stronger (from 9:00 a.m. to 10:30, 100-200W/m^2), the indoor temperatures of cool and dark states are obviously ~2°C lower than low-e glass. Considering the lighting indoor, the cool state is suitable during this time. When the solar irradiance reaches its peak (>600 W/m^2), after 10:30, the indoor temperature of dark state is ~8°C lower than low-e glass. Remarkable, as shown in the inset of Fig. 3b, cool state shows a faster cooling rate than other states at sunset (after 16:30), which indicates that during this time, cool state is more applicable. From an all-year-round perspective, the tri-stable EC window demonstrates superiority by switching among the three states compared with low-e windows in terms of source energy saving.

Thermal modelling and energy-saving evaluation

To further explore the energy-saving performance of the tri-stable ECD, we performed extensive simulations based on the device properties and the climate database. Here, we used EnergyPlus to evaluate HVAC (heating, ventilation, and air-conditioning) energy-saving performance (see Methods for more details). A house with the dimensions of 20*10*3 m and eight 4.5*2 m windows were employed to study the parameters that affect the energy-saving performance of tri-stable EC windows (Supplementary Fig. 22). Here, the indoor air temperature set-point was set constantly as 22 °C. To simulate the lighting environment for human activity, during the night from 23:00 to 7:00, the interiorlight was set constantly as 0 W/m^2; During the daytime, the illuminance setting value is 500 lx. When the daytime illuminance is higher than 500 lx, the lighting power is 0. When the daytime illuminance is lower than 500 lx, the lighting power will increase linearly from 0 to 13 W/m^2.

To obtain the most optimal EC state under different weather conditions, we compared the energy costs among the three optical states around the world cross different climate zones. Among all the three states, we chose the lowest-energy cost state as the final state to be added in the all-year energy statistics. **Fig. 4a** summarized the selections of optical states in different ambient temperatures and solar irradiation densities (Supplementary Fig. 24 for more information). Specifically, at cold weather, the bright state is on, so that both NIR and visible light enter the room; at hot weather, the cool and dark states would be turned on successively according to specific temperature and solar irradiation, so that the NIR and visible light are regulated independently; at night, both NIR and visible light are blocked to prevent privacy (**Fig. 4b**). As shanghai is a large city with great energy consumption, it was chosen as the location of simulation for energy-saving evaluation (More details about the simulation are given in Supplemental Information).[33] As shown in **Fig. 4c**, during the May Day, to get lowest-energy cost state, the EC window is supposed to be switched among three states. It is worthy to note that, considering great tri-stability of the EC device (>4 hour as mentioned in above section), maintaining these states would cost zero energy.

Also taking shanghai as an example, the monthly HVAC energy consumption showed that tri-stable EC window has the lowest energy usage in the whole year (**Fig. 4d**). With the normal glass as the baseline, the tri-band optimized ECD is able to save 23.9% of annual HVAC energy consumption for the whole year, which is the better compared with traditional ECD (~15.5%) and low-E glass (~13.3%) as shown in Supplementary Fig. 25. The simulation results further prove the efficacy of the proposed tri-stable EC window in summer as its suppressed solar transmission. Further simulations in different climates around the world were carried out to evaluate the annual energy-saving performance of the tri-stable EC window across different climate zones. Our tri-stable EC device yielded a higher energy-saving performance benchmarked by a commercial low-E glass across almost all different climates (**Fig. 4e**), with energy saving up to 596.7 MJ m^{-2} (Tennant, AUS, Supplementary Fig. 26), which further shows the potential importance of tri-band regulation in windows.

Conclusion

We have demonstrated that the electrochromic device (ECD) based on a VO_2/WO_3 structure has the ability to dynamically and independently regulate the transmittance of NIR and visible light, exhibiting high coloration efficiencies, fast switching times, and cyclability. Moreover, by utilizing the lower surface potential of the rutile-Li_xVO_2 film, we were able to improve the tri-stability of the ECD to less than 10% in 4 hours. To further enhance the energy-saving performance of the tri-stable ECD, we designed a low-emissivity structure of quartz-ITO/WO_3/VO_2/ SPE/ITO-PE to reduce radiative heat exchange in ambient conditions. This structure features a high-emissivity quartz substrate on the outdoor side and a low-emissivity PE/ITO layer on the indoor side, which effectively minimizes the radiative heat exchange between the indoor and outdoor environments, resulting in energy savings for both cooling and heating throughout the year while maintaining the desired aesthetic effect. Our simulations show that this ECD offers greater energy savings for heating and cooling compared to commercial low-emissivity glass in most climates around the world. These findings provide opportunities for the development of new and efficient smart window designs, as well as applications in information displays and triple-state optical devices.

Figure Captures

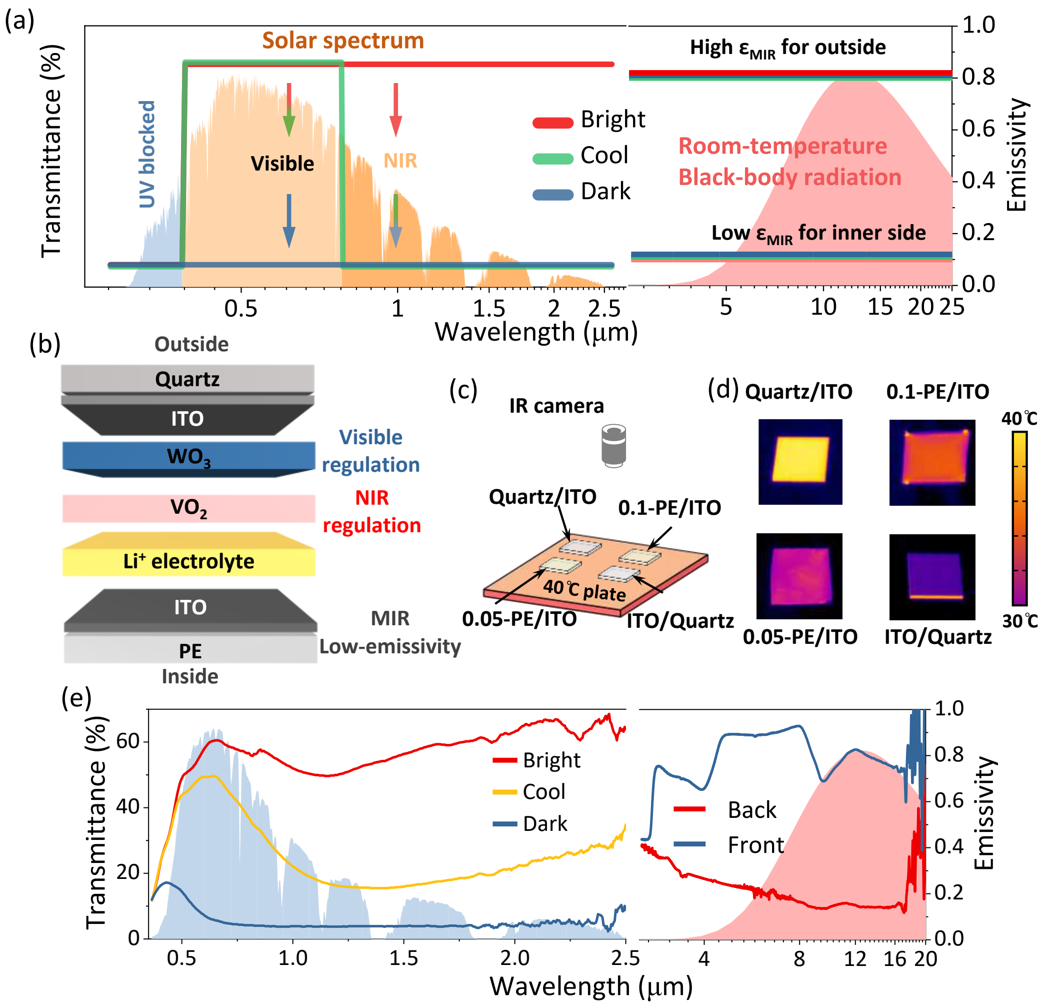

Figure 1. Concept and design of the ECD. (a) Concept of the ideal energy-saving smart window. The red, green, and blue lines represent the spectra for an ideal smart window. Spectra of solar irradiation (plotted by AM 1.5G, global tilt) and room-temperature thermal radiation simulated using Planck's law at 300 K are plotted for reference. **(b)** Schematics of the optimizing-multispectral EC device with low-emissivity surface. **(c)** Schematic of the experiment examining the surface temperatures of samples on a hot stage. **(d)** Thermal images of the quartz/ITO, 0.1mm-PE/ITO, 0.05mm-PE/ITO and ITO/quartz on the same hot stage. **(e)** Transmittance spectra (0.35-2.5 μm) the optimizing-multispectral EC device at Bright (+1.5 V), Cool (-1.5 V) and Dark (-3.0 V) states, and LWIR emissivity (2.5-20 μm) of the front/back faces.

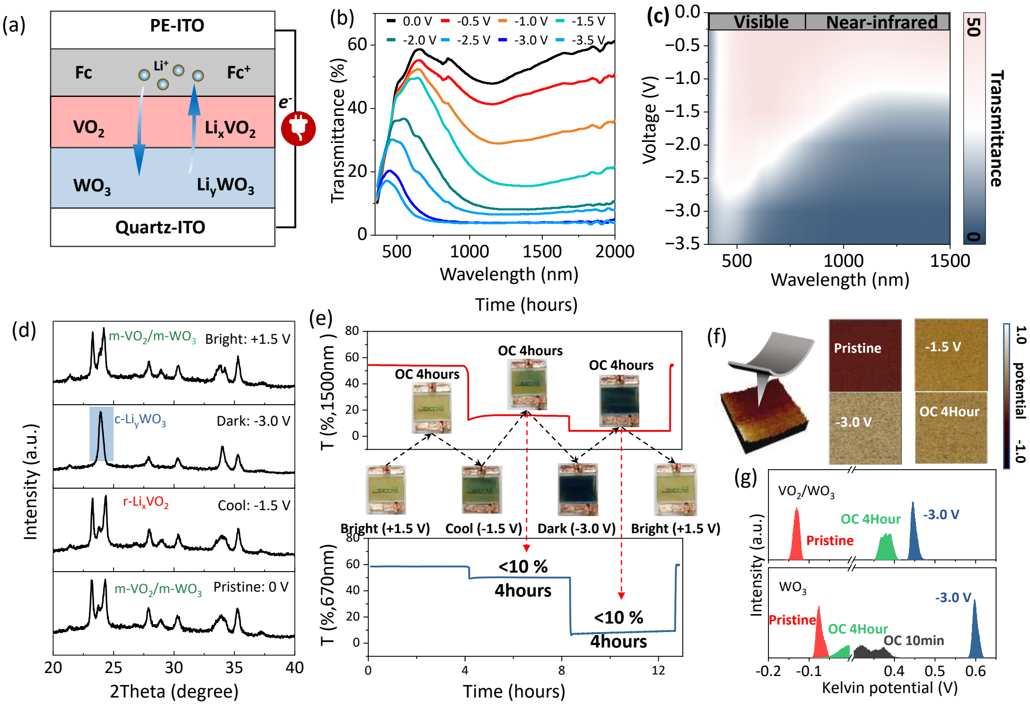

Figure 2. Characteristic of the tri-stable ECD. (a) Schematic structure and internal ionic diffusion of the EC device. **(b)** Transmittance spectra of the dual-band ECD under voltages from 0 V to -3.5 V. **(c)** The transmittance contour-map of the EC device under different voltages applied for converted from the measured transmittance spectra. **(d)** *ex-situ* XRD patterns of VO_2/WO_3 at pristine state and at -1.5, -3.0 and +1.5 V bias voltages. **(e)** The transmittance changes at 670 nm (bottom) and 1500 nm (upper) of VO_2/WO_3 (orange line) devices during open circuit (OC) after the film was biased at +1.5 V, -1.5 V and -3.0 V for 20 s. The inset is the real-photo of VO_2/WO_3 EC device during the coloration-bleaching process. The kelvin potential mapping **(f)** of VO_2/WO_3 and relative potential counts **(g)** of VO_2/WO_3 and WO_3 under bias voltage conditions of 0 V, -1.5 V, -3.0 V and open circuit for 4 hours.

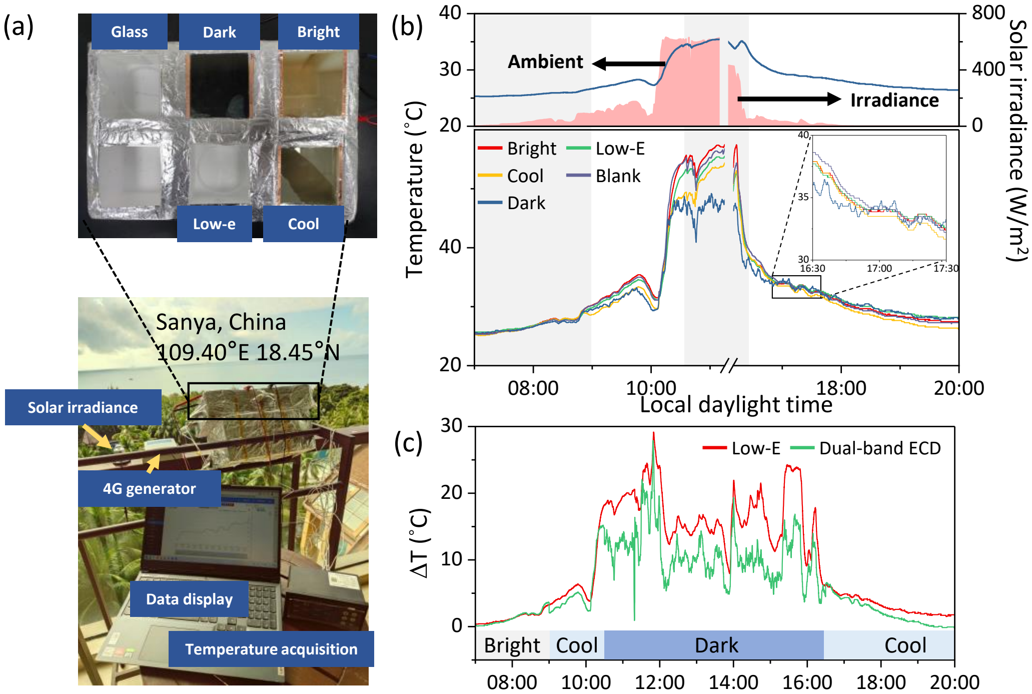

Figure 3. Outdoor performance of the tri-stable ECD. (a) Photographs of the measuring setup performed in the balcony of a house at Sanya, China and the five experimental windows: tri-stable ECD with bright, cool, dark states, commercial low-e glass and white glass. **(b)** Real-time room temperatures with five experimental windows. Upper part: ambient temperature (blue, left y-axis) and real-time solar irradiance (red pattern, right y-axis). **(c)** Temperature difference between the ambient surroundings and the experimental windows. The tri-stable ECD works as followed ways: 00:00-9:00, bright state; 9:00-10:30 and 16:30-20:00, cool state; 10:30-16:30, dark state.

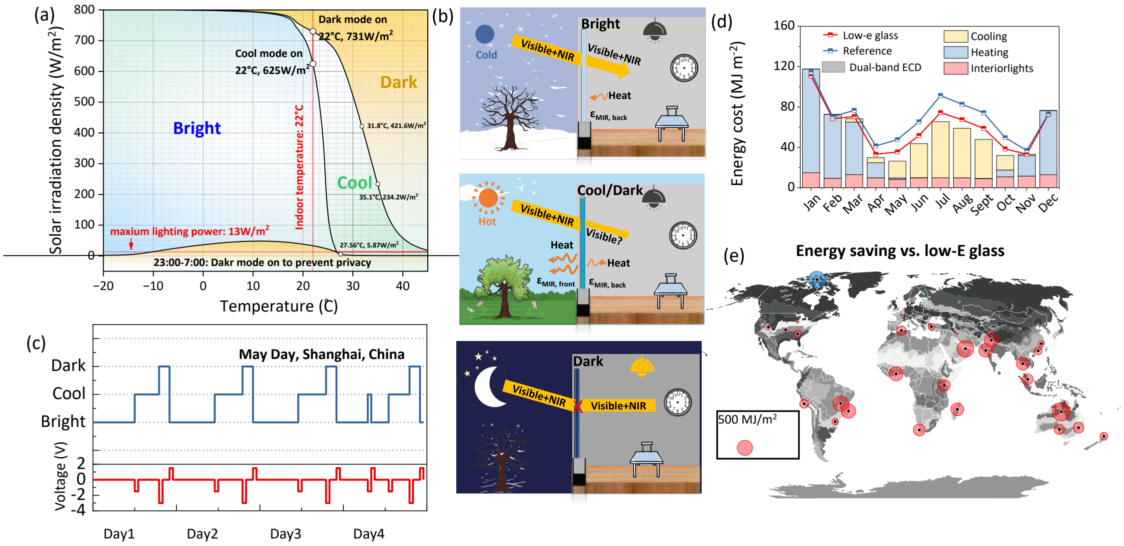

Figure 4. Energy-saving evaluation of tri-stable ECD. (a) Selections of optical states according to different weather conditions by Energy-plus simulation (more details are given in Supplementary information). Different region represents the lowest energy state at the current temperature and irradiation. (Blue: Bright state; Green: Cool; Yellow: Dark state). **(b)** Switching of optical states (top) and bias voltages (bottom) for energy-saving in Shanghai during May Day. **(c)** Working principle of the EC window at cold weather (top) and hot weather (medium) and night (bottom). The yellow arrows indicate the solar irradiation, and the orange arrows represent heat radiation. At cold weather, both NIR and visible light enter the room. At hot weather, NIR and visible light are regulated independently according to specific temperature and solar irradiation. At night, both NIR and visible light are blocked to prevent privacy. **(c)** Monthly energy consumption of the EC device, low-E glass, and normal glass window in the climate condition of Shanghai. **(e)** Estimated heating and cooling energy-saving of a tri-stable EC device against a commercial low-E glass as the baseline for different cities representing different climate zones. Unit for the energy-saving is MJ m^{-2}.

Data Availability Statement

The data that support the findings of this study are available from the corresponding author upon reasonable request.

Acknowledgments

This study was financially supported by the National Key Research and Development Program of China (no. 2021YFA0718900), the Key Collaborative Research Program of the Alliance of International Science Organizations (no. ANSO-CR-KP-2021-01); the National Natural Science Foundation of China (nos. 51972328, 62005301, 52002392 and 62175248); Shanghai B&R International Cooperation Program (no. 20640770200); Shanghai 'Science and Technology Innovation Action Plan' Intergovernmental International Science and Technology Cooperation Program (no. 21520712500); Shanghai Science and Technology Funds (no. 23ZR1481900); the Open Project of Wuhan National Laboratory for Optoelectronics (no. 2022WNLOKF014); Science Foundation for Youth Scholar of State Key Laboratory of High Performance Ceramics and Superfine Microstructures (no. SKL202202).

Author Contributions Statement

X.C. conceived the project. Z.S., X.C. and A.H. designed the experiments and analyzed the data. Z.S., X.J., and A.H. performed the experiments and some characterizations. Z.S., C.C., W.H. and R.Y. performed optical simulations under the supervision of P.J., J.B. and H.L. X.C. and Z.S. conceived the device working mechanism, conducted the computational studies and data analysis. Z.S. and R.Y. wrote the paper. All authors discussed the results and commented on the manuscript.

Competing Interests Statement

The authors declare no competing financial interest.

Reference

1. Zhao, L.; Lee, X.; Smith, R. B.; Oleson, K., Strong contributions of local background climate to urban heat islands. *Nature* **2014,** *511* (7508), 216-219.
2. Cuce, E.; Riffat, S. B., A state-of-the-art review on innovative glazing technologies. *Renewable and sustainable energy reviews* **2015,** *41*, 695-714.
3. Gao, Y.; Wang, S.; Luo, H.; Dai, L.; Cao, C.; Liu, Y.; Chen, Z.; Kanehira, M., Enhanced chemical stability of VO 2 nanoparticles by the formation of SiO 2/VO 2 core/shell structures and the application to transparent and flexible VO 2-based composite foils with excellent thermochromic properties for solar heat control. *Energy & Environmental Science* **2012,** *5* (3), 6104-6110.
4. Shao, Z.; Huang, A.; Ming, C.; Bell, J.; Yu, P.; Sun, Y.-Y.; Jin, L.; Ma, L.; Luo, H.; Jin, P., All-solid-state proton-based tandem structures for fast-switching electrochromic devices. *Nature Electronics* **2022**, 1-8.
5. Barawi, M.; De Trizio, L.; Giannuzzi, R.; Veramonti, G.; Manna, L.; Manca, M., Dual band electrochromic devices based on Nb-doped TiO2 nanocrystalline electrodes. *ACS nano* **2017,** *11* (4), 3576-3584.
6. Zhai, Y.; Li, J.; Shen, S.; Zhu, Z.; Mao, S.; Xiao, X.; Zhu, C.; Tang, J.; Lu, X.; Chen, J., Recent Advances on Dual-Band Electrochromic Materials and Devices. *Advanced Functional Materials* **2022**, 2109848.
7. Zhang, S.; Cao, S.; Zhang, T.; Fisher, A.; Lee, J. Y., Al 3+ intercalation/de-intercalation-enabled dual-band electrochromic smart windows with a high optical modulation, quick response and long cycle life. *Energy & Environmental Science* **2018,** *11* (10), 2884-2892.
8. Wen, R.-T.; Granqvist, C. G.; Niklasson, G. A., Eliminating degradation and uncovering ion-trapping dynamics in electrochromic WO3 thin films. *Nature materials* **2015,** *14* (10), 996-1001.
9. Islam, S. M.; Hernandez, T. S.; McGehee, M. D.; Barile, C. J., Hybrid dynamic windows using reversible metal electrodeposition and ion insertion. *Nature Energy* **2019,** *4* (3), 223-229.
10. Chen, J.; Wang, Z.; Chen, Z.; Cong, S.; Zhao, Z., Fabry–Perot cavity-type electrochromic supercapacitors with exceptionally versatile color tunability. *Nano Letters* **2020,** *20* (3), 1915-1922.
11. Liu, B. J.-W.; Zheng, J.; Wang, J.-L.; Xu, J.; Li, H.-H.; Yu, S.-H., Ultrathin W18O49 nanowire assemblies for electrochromic devices. *Nano letters* **2013,** *13* (8), 3589-3593.
12. Cheng, W.; He, J.; Dettelbach, K. E.; Johnson, N. J.; Sherbo, R. S.; Berlinguette, C. P., Photodeposited amorphous oxide films for electrochromic windows. *Chem* **2018,** *4* (4), 821-832.
13. Zhang, S.; Cao, S.; Zhang, T.; Yao, Q.; Fisher, A.; Lee, J. Y., Monoclinic oxygen-deficient tungsten oxide nanowires for dynamic and independent control of near-infrared and visible light transmittance. *Materials Horizons* **2018,** *5* (2), 291-297.
14. Gu, H.; Guo, C.; Zhang, S.; Bi, L.; Li, T.; Sun, T.; Liu, S., Highly efficient, near-infrared and visible light modulated electrochromic devices based on polyoxometalates and W18O49 nanowires. *ACS nano* **2018,** *12* (1), 559-567.
15. Heo, S.; Kim, J.; Ong, G. K.; Milliron, D. J., Template-free mesoporous electrochromic films on flexible substrates from tungsten oxide nanorods. *Nano letters* **2017,** *17* (9), 5756-5761.
16. Wang, S.; Jiang, T.; Meng, Y.; Yang, R.; Tan, G.; Long, Y., Scalable thermochromic smart windows with passive radiative cooling regulation. *Science*, **2021**, 374(6574): 1501-1504.
17. Tang, K.; Dong, K.; Li, J.; Gordon, M. P.; Reichertz, F. G.; Kim, H., ... & Wu, J. Temperature-adaptive radiative coating for all-season household thermal regulation. *Science,* **2021**, *374*(6574), 1504-1509.

18. Peng, Y.; Fan, L.; Jin, W.; Ye, Y.; Huang, Z.; Zhai, S.; ... & Cui, Y. Coloured low-emissivity films for building envelopes for year-round energy savings. *Nature Sustainability*, **2022**, *5*(4), 339-347.

19. Mandal, J.; Du, S.; Dontigny, M.; Zaghib, K.; Yu, N.; Yang, Y., $Li_4Ti_5O_{12}$: A visible-to-infrared broadband electrochromic material for optical and thermal management. *Advanced Functional Materials* **2018**, 28(36), 1802180.

20. Ergoktas, M. S.; Bakan, G.; Kovalska, E.; Le Fevre, L. W.; Fields, R. P.; Steiner, P.; ... & Kocabas, C.; Multispectral graphene-based electro-optical surfaces with reversible tunability from visible to microwave wavelengths. *Nature photonics* **2021** 15(7), 493-498.

21. Rao, Y.; Dai, J.; Sui, C.; Lai, Y. T.; Li, Z.; Fang, H.; ... & Hsu, P. C., Ultra-Wideband Transparent Conductive Electrode for Electrochromic Synergistic Solar and Radiative Heat Management. *ACS Energy Letters* **2021**, 6(11): 3906-3915.

22. Sui, C., Pu, J., Chen, T. H., Liang, J., Lai, Y. T., Rao, Y., ... & Hsu, P. C. Dynamic electrochromism for all-season radiative thermoregulation. *Nature Sustainability*, **2023** 1-10.

23. Ke, Y.; Chen, J.; Lin, G.; Wang, S.; Zhou, Y.; Yin, J.; Lee, P. S.; Long, Y., Smart windows: electro-, thermo-, mechano-, photochromics, and beyond. *Advanced Energy Materials* **2019,** *9* (39), 1902066.

24. Nakano, M.; Shibuya, K.; Okuyama, D.; Hatano, T.; Ono, S.; Kawasaki, M.; Iwasa, Y.; Tokura, Y., Collective bulk carrier delocalization driven by electrostatic surface charge accumulation. *Nature* **2012,** *487* (7408), 459-462.

25. Jeong, J.; Aetukuri, N.; Graf, T.; Schladt, T. D.; Samant, M. G.; Parkin, S. S., Suppression of metal-insulator transition in VO2 by electric field–induced oxygen vacancy formation. *Science* **2013,** *339* (6126), 1402-1405.

26. Xu, J.; Zhang, Y.; Zhai, T.-T.; Kuang, Z.; Li, J.; Wang, Y.; Gao, Z.; Song, Y.-Y.; Xia, X.-H., Electrochromic-tuned plasmonics for photothermal sterile window. *ACS nano* **2018,** *12* (7), 6895-6903.

27. Kim, Y.; Cha, S.; Kim, J.-H.; Oh, J.-W.; Nam, J.-M., Electrochromic response and control of plasmonic metal nanoparticles. *Nanoscale* **2021,** *13* (21), 9541-9552.

28. Lee, S.-H.; Seong, M. J.; Cheong, H. M.; Ozkan, E.; Tracy, E. C.; Deb, S. K., Effect of crystallinity on electrochromic mechanism of LixWO3 thin films. *Solid State Ionics* **2003,** *156* (3-4), 447-452.

29. Brezesinski, T.; Fattakhova Rohlfing, D.; Sallard, S.; Antonietti, M.; Smarsly, B. M., Highly crystalline WO3 thin films with ordered 3D mesoporosity and improved electrochromic performance. *Small* **2006,** *2* (10), 1203-1211.

30. Chen, Y.; Wang, Z.; Chen, S.; Ren, H.; Wang, L.; Zhang, G.; Lu, Y.; Jiang, J.; Zou, C.; Luo, Y., Non-catalytic hydrogenation of VO2 in acid solution. *Nature communications* **2018,** *9* (1), 1-8.

31. Chen, S.; Wang, Z.; Ren, H.; Chen, Y.; Yan, W.; Wang, C.; Li, B.; Jiang, J.; Zou, C., Gate-controlled VO2 phase transition for high-performance smart windows. *Science advances* **2019,** *5* (3), eaav6815.

32. Chen, Y.; Wang, Z.; Chen, S.; Ren, H.; Li, B.; Yan, W.; Zhang, G.; Jiang, J.; Zou, C., Electric-field control of Li-doping induced phase transition in VO2 film with crystal facet-dependence. *Nano Energy* **2018,** *51*, 300-307.

33. Edition, S.; Erbe, D.; Lane, M.; Anderson, S.; Baselici, P.; Hanson, S.; Heinisch, R.; Humble, J.; Taylor, S.; Kurtz, R., Energy standard for buildings except low-rise residential buildings. **2010**.

Supplementary Files

This is a list of supplementary files associated with this preprint. Click to download.

- supplementalinformation.pdf